Modelling of glass moulding, in particular small scale surface changes

EINDHOVEN UNIVERSITY OF TECHNOLOGY
Department of Mathematics and Computing Science

RANA 96–11
July 1996

Modelling of glass moulding, in particular small scale surface changes

by

S.L. de Snoo
R.M.M. Mattheij
G.A.L. van de Vorst

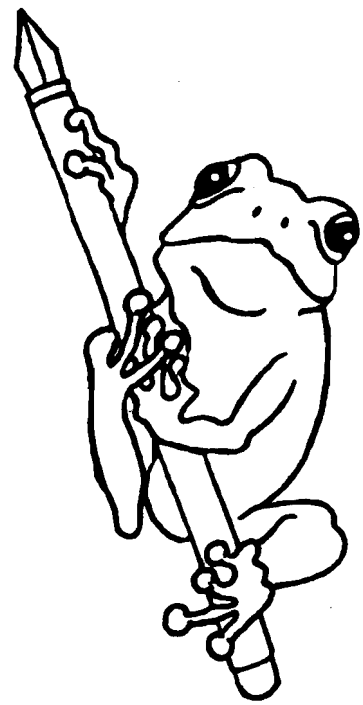

Reports on Applied and Numerical Analysis
Department of Mathematics and Computing Science
Eindhoven University of Technology
P.O. Box 513
5600 MB Eindhoven
The Netherlands
ISSN: 0926–4507

Modelling of glass moulding, in particular small scale surface changes

S.L. de Snoo[†], *R.M.M. Mattheij*[†] *and G.A.L. van de Vorst*[‡]

[†] Department of Mathematics, Eindhoven University of Technology, The Netherlands

[‡] Institute for Agrotechnological Research (ATO-DLO) Wageningen, The Netherlands

Abstract

In this paper we give an interesting example of glass modelling, viz. the morphology of small glass dimples in a mould before and after pressure. We derive a mathematical model with suitable boundary conditions and solve the two problems by a finite element and a boundary element technique respectively. We give a number of examples illustrating the analysis.

1 Introduction

For many years glass technology has been a craft based on expertise and experimental knowledge, reasonably sufficient to keep the products and the production competitive. Over the last twenty years mathematical modelling of the various aspects of the production has become increasingly decisive, however. This is induced in part by fierce competition from other materials notably polymers, which e.g. have found their corner in the food packing industry. For another part this is a consequence of environmental concerns. It is not so much the waste (glass is 100% recyclable, a strong advantage to most other competitors) as the energy consumption. One should realise that the melting process of sand to liquid glass makes up for the largest cost factor of the product. To give an idea of the relative importance of the industry nowadays some figures: In the European Union about 25 Megaton of glass is being produced, which represents 30 billion dollars worth. The industry

employs over 200,000 people. The figures in the United States are comparable. Two thirds of the glass production is meant for packing ("jars and bottles"). Float glass (as used for panes) makes up for one quarter. The rest is for special products like CRTs and fibres.

The production of glass forms goes more or less along the following lines: First grains and additives, like soda, are being heated in a tank. This can be a device several tens of metres long and a few metres high and wide (width being larger than height). Here gas burners or electric heaters provide for the heat necessary to warm up the material till some 1200°C. At one end the liquid glass comes out and is led to the pressing or blowing machine, or ends up on a bed of liquid tin, where it spreads out to become float glass (for pane, wind shields etc.). To obtain a glass form often a two-stage process is being used: first a blob of hot glass is pressed into a mould to form a so called *parison*. Here it is cooled down (the mould is kept at 500°C) such that a small skin of solid glass is formed. This parison is then blown into its final shape. Such a pressing/blowing machinery can produce a number of products at the same time; as a result a more or less steady flow of glass products is coming out on a belt, which then have to be cooled down further in a controlled way such that the remaining stresses are as small as possible (and thus the strength is optimal).

Sometimes only pressing is needed. This is the case in the production of CRTs. Here a stamp is pressed into liquid glass and after lifting it again a certain morphology should have been transferred onto the glass screen. We shall consider two problems arising in this process. One is how small dimples (app. 1 μm) in the mould are being filled by the liquid glass during the pressing phase. The other problem is how their glassy counterparts are smoothed out after the mould has been withdrawn. The modelling and simulation is important for the manufacturer as these small dimples are needed for letting fluorescent dyes stick sufficiently well.

This paper is organised as follows: First we derive a mathematical model for the glass flow. This is done in §2, where we shall investigate the characteristics of the flow, resulting in a Stokes equation. The latter equation combined with suitable boundary conditions is used to simulate the flow of the two processes mentioned above. Although the temperature plays a crucial role in the morphology (the shape is retained only after suitable cooling has taken place), we shall restrict ourselves to isotherm situations here. The simulation of the flow after the stamp has been lifted is done first. In §3 we employ a boundary element method for solving the (Neumann type) free boundary value problem

for some model configuration. The actual pressing is simulated, again for a model problem, in §4, where we use a finite element method.

2 The model equations

In this section we shall give a mathematical model describing the glass flow. Since our actual problem (the small dimple rheology) takes place on a micrometer scale, we need to assess the dimensionless quantities before proceeding to simulating these flows numerically. For the two afore mentioned problems we shall simplify our model further and consider the morphology of just a small drop. This simplification is done in order to compare the results with existing analytical approximations, thus illustrating their accuracy.

The motion of glass at temperatures above $600°C$ can be described by the Navier-Stokes equation for incompressible Newtonian fluids,

$$Re\left(Sr\frac{\partial \bar{\mathbf{u}}}{\partial \bar{t}} + (\bar{\mathbf{u}}\cdot\nabla)\bar{\mathbf{u}} \right) = -\nabla\cdot\bar{\sigma} + \frac{Re}{Fr}\bar{g}\,. \tag{2.1}$$

Here $\bar{\mathbf{u}}$ is the dimension free velocity, $\bar{t}$ the dimension free time, $\bar{g}$ the dimension free gravity and

$$\bar{\sigma} = \left(\nabla\bar{\mathbf{u}} + \nabla\bar{\mathbf{u}}^{T}\right) - \bar{p}\mathbf{I}\,, \tag{2.2}$$

the dimension free stress tensor, with the dimension free pressure $\bar{p}$. *Re*, *Sr* and *Fr* are the *Reynolds*, *Froude* and *Strouhal* numbers respectively, which characterise the flow. These numbers are expressed in the characteristic parameters of the flow. Using a pressure p_c and a length l_c, characteristic for the manufacturing process, and a typical density ρ and a viscosity μ, for glass at a the processing temperature, a characteristic velocity

$$u_c = \frac{p_c l_c}{\mu} \tag{2.3}$$

and a characteristic time scale

$$t_c = \frac{l_c}{u_c} = \frac{\mu}{p_c}\,, \tag{2.4}$$

are found and the dimension free numbers are

$$Re = \frac{\rho l_c u_c}{\mu} = \frac{\rho p_c l_c^2}{\mu^2}\,, \quad Fr = \frac{u_c^2}{g l_c} = \frac{p_c^2}{g\mu^2}\,, \quad Sr = \frac{t_c l_c}{u_c} = 1\,, \tag{2.5}$$

with g the gravitational acceleration.

A typical value for the pressure during the moulding process is $10^5\ N/m^2$. The length scale of the surface variations of interest in is $10\ \mu m$. The density of glass is $2500\ kg/m^3$ cf. [29]. The viscosity of glass strongly depends on the temperature. At $600°C$ the viscosity is $10^{12}\ N\,s/m^2$. At 700, 800 and $900°C$ one finds 4.10^8, 4.10^6 and $2.10^5\ kg\,s/m^2$ respectively. The Reynolds number for such a flow varies from 10^{-26} to 10^{-13}, and the quotient Re/Fr is of about 10^{-11}. Inertial and gravitational effects can thus be neglected.

The motion of the fluid can thus be described adequately by the stationary Stokes-equations for incompressible fluids

$$\nabla \cdot \bar{\sigma} = 0, \tag{2.6}$$

$$\nabla \cdot \bar{\mathbf{u}} = 0. \tag{2.7}$$

The surface tension provides for the boundary conditions on the free surface

$$\sigma \mathbf{n} = (\kappa\gamma - P_{ext})\mathbf{n}. \tag{2.8}$$

Here κ is the curvature of the surface, γ the surface tension and P_{ext} the external pressure. In dimension free quantities this reads

$$\bar{\sigma}\mathbf{n} = \left(\frac{1}{Ca}\bar{\kappa} - \bar{P}_{ext}\right)\mathbf{n}, \tag{2.9}$$

with

$$Ca := \frac{u_c \mu}{\gamma} = \frac{p_c l_c}{\gamma}, \tag{2.10}$$

the so called *capillary* number.

As remarked above we will consider the spreading of a small drop on a solid surface as being typical for the phenomenon we are interested in. Hence we take the size of the drop equal to the typical length scale of $10\ \mu m$. The pressure in a stationary drop equals

$$p = 2\frac{\gamma}{r}, \tag{2.11}$$

with r the radius of the drop. The surface tension of glass equals $0.3\ N/m$. The pressure in a $10\ \mu m$ drop is thus about $10^5\ N/m^2$, as was the pressure in the mould.

A major point of interest in the study of the evolution of a viscous blob under surface tension is the range of time scales present in the problem. These time scales can be found from a dimension analysis. A non-dimensional formulation

based on the characteristic length l_c, surface tension γ, and viscosity μ this implies a characteristic velocity

$$u_c = \frac{\gamma}{\mu}, \tag{2.12}$$

and a characteristic time scale

$$t_c = \frac{l_c}{u_c} = l_c \frac{\mu}{\gamma}. \tag{2.13}$$

At first sight it may seem strange that the characteristic velocity does not depend on the characteristic length scale. To understand this a sinusoidal perturbation of the surface can be considered. The velocity of the surface will be proportional to the ratio of the magnitude and the wavelength of the sinus and thus be independent of the characteristic length. The length scale of the geometry does not influence the velocity. On the other hand the characteristic time is proportional to the characteristic length. As a consequence smaller geometries will evolve faster. Under the influence of surface tension, perturbations of the surface with a short wavelength will smooth out quickly. The longer time scales in a geometry will thus be more or less proportional to the largest length scale and the shorter time scales to the smallest length scales, which is zero in the continuous case and equal to the length scale of discretisation in the discrete case. This wide range of time scales may result in a stiff problem, when solving the differential equations numerically.

3 Deformation of a glass drop on a glass surface

The simplest of the two problems mentioned in the introduction is the deformation of the little glass peak left by a dimple in the mould after it has been withdrawn. In reality one should expect a thin skin of cool glass covering a rather non-isothermal glass body. Yet we shall treat it as isothermal for simplicity. In its most simplified form the geometry can be seen as a plate coalescing with a ball (or a cylinder in a typical 2D setting). This in turn is not so much different from the sintering of two spheres (or cylinders), which was extensively studied in [31]. The mathematical problem can be formulated as a Stokes equation with a Neumann boundary, viz. the free surface energy.

Since this problem essentially deals with the displacement of the boundary only it is ideally suited for a boundary element approach (BEM). We shall first outline the numerical method in §3.1. In §3.2 we shall discuss some simulation results.

3.1 Numerical Solution Method

We start by outlining the solution method for the simulation of the deformation of a two-dimensional profile; the axisymmetric case will be discussed at the end of this section. As mentioned above, the Stokes' flow on the halfspace is solved by a BEM, which yields the boundary velocity field at a fixed time, in combination with a time integration method. The BEM is applied to the integral formulation for the Stokes problem based on the hydrodynamical single- and double-layer potentials. In the two-dimensional case, this formulation reads for a particular point ($\mathbf{x}$) on the boundary of the halfspace (Γ),

$$\frac{1}{2}v_i(\mathbf{x})+\int_\Gamma q_{ij}(\mathbf{x}-\mathbf{y})v_j(\mathbf{y})\,d\Gamma_y=\int_\Gamma u_{ij}(\mathbf{x}-\mathbf{y})b_j(\mathbf{y})\,d\Gamma_y. \tag{3.1}$$

Here the vectors $\mathbf{v}$ and $\mathbf{b}$ denote the velocity and surface tension respectively. The latter is equal to

$$\mathbf{b}(\mathbf{x})=\kappa(\mathbf{x})\mathbf{n}(\mathbf{x}), \tag{3.2}$$

where κ is the boundary curvature and $\mathbf{n}$ the outward normal vector. The kernels q_{ij} and u_{ij} in equation (3.1) are equal to

$$q_{ij}(\mathbf{r})=\frac{r_i r_j}{\pi R^2}r_k n_k, \qquad u_{ij}(\mathbf{r})=\frac{1}{4\pi}\left[-\delta_{ij}\log R+\frac{r_i r_j}{R^2}\right], \tag{3.3}$$

respectively, where $R=|\mathbf{r}|=\sqrt{r_1^2+r_2^2}$.

Generally, the Boundary Element Method consists of dividing the boundary curve into elements which are defined by a set of nodal points, say N in total. Then, on each element the velocity and tension are approximated by Lagrangian interpolation polynomials of degree one less than the number of nodes needed to describe a single element. Substitution of these polynomials into the integral equation (3.1) subjected to the discretized boundary curve and an arbitrary collocation point yields two linear algebraic equations for the 2N unknown nodal velocities. If we vary the collocation point in these equations over all the nodes, a square full rank system of 2N linear algebraic for the unknown velocity field is obtained. More about the implementation of the BEM can be found in Banerjee [2], Becker [4] and Brebbia *et al.* [7].

The BEM solution described above, applies for domains with a closed boundary curve; in the case of a halfspace, the infinite part of the boundary has to be treated in a special way. A solution method, suggested by Beer and Watson [5], is the introduction of so-called *infinite boundary elements*: the infinite boundary part is considered as one element. To implement the infinite

shape functions, one applies the usual quadratic polynomials, by taking the limits of the intrinsic variable, say s, equal to -1 to ∞ instead of -1 to +1. In order to apply a Gaussian quadrature formula for the numerical integration of the thus obtained infinite integral, the integration limits have to lie between -1 and +1. This is easily achieved by a suitable substitution for the integration variable. Finally, the velocity and tension have to obey the decay conditions at infinity. This is performed by the assumption that their variations over the infinite elements are as follows,

$$v_i(\mathbf{x}) = \frac{|\mathbf{x}_0 - \mathbf{x}(-1)|}{|\mathbf{x}_0 - \mathbf{x}(s)|} v_i(-1), \qquad b_i(\mathbf{x}) = \frac{|\mathbf{x}_0 - \mathbf{x}(-1)|^2}{|\mathbf{x}_0 - \mathbf{x}(s)|^2} b_i(-1), \tag{3.4}$$

where $-1 \le s \le \infty$ and $\mathbf{x}_0$ is an arbitrary reference point in the fluid. Note that $\mathbf{v}(-1)$ and $\mathbf{b}(-1)$ represent the velocity and the tension of the first unknown. It appears that the same decay functions can be applied in the three-dimensional case.

In Hopper [19], it is shown that the shape function of the coalescence of a cylinder on a halfspace can be described by

$$x_1(x_2, h) = \pm \frac{\left(1 + 4hx_2 - h^2\right)\sqrt{h - x_2}}{4h\sqrt{x_2}}, \tag{3.5}$$

where h is the maximum height of the shape, i.e. a function of the time t. Employing an asymptotic expansion for $x_2 \to 0$ of equation (3.5) up to the second order yields,

$$x_1 = \pm\left[\frac{1 - h^2}{4\sqrt{hx_2}} + O\left(\sqrt{x_2}\right)\right], \quad \text{hence } x_2 \approx \frac{\left(1 - h^2\right)^2}{16hx_1^2}. \tag{3.6}$$

Let the truncation point be denoted by $\mathbf{a}$, then for the infinite boundary shape we obtain by substitution of equation (3.6) the following approximate expression

$$x_2 = a_2 \frac{x_2}{a_2} = \frac{a_2 a_1^2}{x_1^2}, \tag{3.7}$$

which is *independent* of h.

In the case of the axisymmetric implementation, we cannot derive such an analytical expression, simply because this problem cannot be solved analytically. Therefore, we apply a simpler method which has already proven its usefulness in the past: the boundary element mesh is truncated at a sufficiently large distance from the region of interest. This approach for the

axisymmetric case has extensively been outlined by Lee and Leal [23]; they simulate the interface deformation caused by the rising of a spherical particle.

After solving the BEM formulation for a fixed domain, a time step has to be carried out. The motion of the boundary is described by the application of the Lagrangian representation for the boundary velocity **v**, i.e.

$$\frac{d\mathbf{x}}{dt} = \mathbf{v}(\mathbf{x}) \qquad (x \in \Gamma). \tag{3.8}$$

Applying the above equation for the system obtained by the BEM discretization yields a system of non-linear Ordinary Differential Equations (ODEs). Since it appears that this system of ODEs can be *stiff* for certain type of shapes (e.g. fluid regions which are having cusp-like regions), we have implemented a variable step, variable order Backward Differences Formulae (BDF) method to solve these ODEs. More details about this implementation are available in Van de Vorst [31].

3.2 Numerical Results

The numerical solution technique outlined in the previous section is tested by

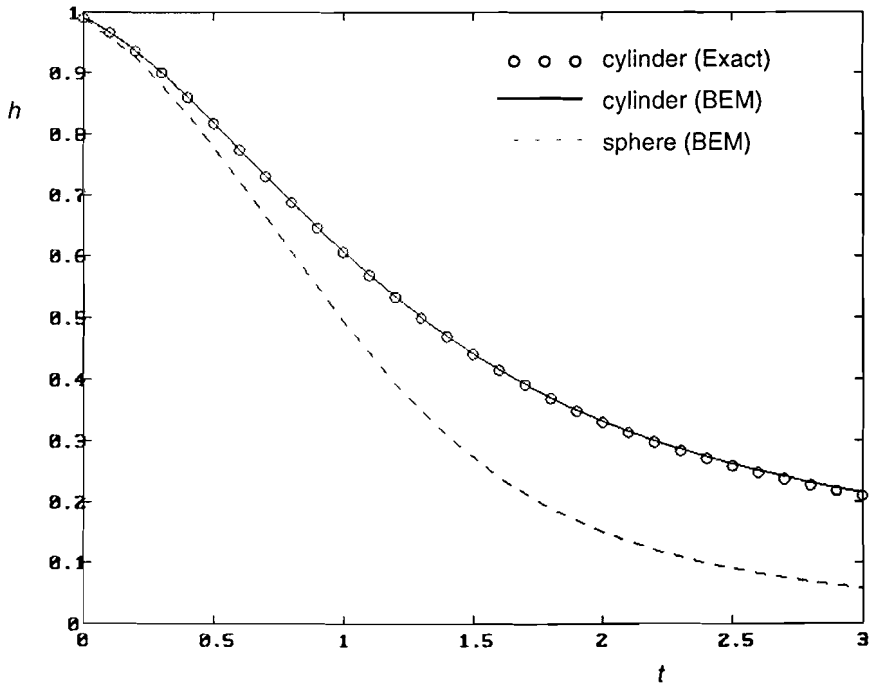

Figure 1: An excellent equivalence is obtained when the analytical (exact) height *h* of the coalescing cylinder is compared to the numerical solution. Moreover, the difference in the height development is compared to the coalescence of a sphere with the same initial radius.

comparing the numerical results with a problem which can be solved analytically: the coalescence of a cylinder on a halfspace. The analytical solution of this problem is found by a conformal mapping technique which is described in Hopper [19]. We compare the development of the height h of the cylinder in time. For the initial geometry we have taken a cylinder with radius equal to 0.5, hence $h = 1$ initially. Since the numerical code requires an initial contact between the halfspace and cylinder, we use the analytical solution curve for $h = 0.99$ as initial shape. Moreover, the halfspace is truncated between -3 and 3.

In figure 1 we have plotted by a solid line the numerically obtained decrease of the height h; the analytical solution is denoted by bullets. It can be observed that an excellent matching is obtained between the numerical and analytical solution for h during a large period of time. In the end a small, but acceptable, error occurs, due to the fact that the approximate shape of the infinite part becomes worse. Also plotted, by a dashed line, is the numerically obtained height development when the initial shape is used in the axisymmetric code: the coalescence of a sphere with initial radius 0.5 on a halfspace. When both evolutions of the height are compared, it can be seen that during the initial stage the deformation proceeds at a similar rate; during later stages the height of the

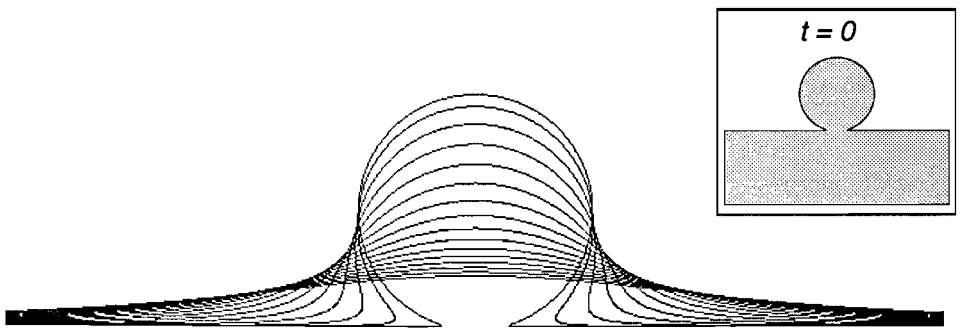

Coalesence of a cylinder with radius 0.5 on a halfspace

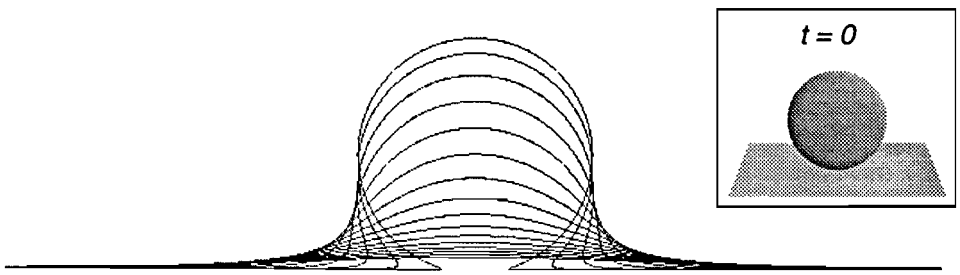

Coalesence of a sphere with radius 0.5 on a halfspace

Figure 2: A comparison between the coalescence of a cylinder on a plate and the coalescence of a sphere with both equal radius of 0.5 for t = 0.0(0.2)3.0

sphere decreases much faster, due to the fact that the fluid flows circulary around the sphere, while in the two-dimensional case there is a planar flow field only. This behaviour can also be observed in figure 2 which shows the shape evolution at subsequent time stages $t = 0.0(0.2)3.0$. The latter two problems relate to a physical problem; it turns out that these solutions can be used to determine the surface tension of a certain glass at relative low temperatures (600°C), cf. De With and Corbijn [34].

4 Deformation of a glass drop on a solid surface

The most important problem met in the morphology transfer is how the geometry of the mould is actually adopted by the liquid glass during the pressing phase. As before we shall consider a typical situation only, as this will give sufficient insight into the general problem, (which is essentially not more difficult numerically). We shall pay some special attention to the modelling of the contact line (§4.1) and then to the numerical method (§4.2). In §4.3 we illustrate this with some numerical simulations.

4.1 Modelling the contact angle

Consider now a blob of moving glass confined by some solid boundary. The place where fluid-solid and fluid-gas interfaces meet is called the *contact line* (which is a single point in a 2D or axisymmetric simulation). On this line the two interfaces form an angle, the contact angle (see figure 3). The influence of the contact angle on fluid flow with a free boundary was first analysed by West in 1912 [33]. For a moving capillary with diameter a, he found a pressure drop (p) between the gas in front of the meniscus and the liquid at a distance L behind the meniscus to be given by

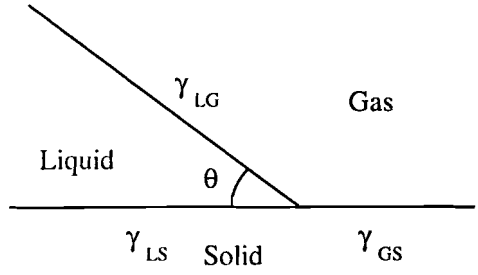

Figure 3: the contact angle θ.

$$p = 8\mu U\frac{L}{a^2} - 2\frac{\gamma}{a}\cos\theta\,, \tag{4.1}$$

with U the velocity of the contact line and θ the contact angle. In a stationary situation the velocity of the contact line is equal to the characteristic velocity u_c. Furthermore, if the distance L equals the diameter a, then

$$p = 8\frac{\gamma}{l_c}\left(Ca - \frac{\cos\theta}{4}\right). \tag{4.2}$$

This analysis shows that both the surface tension and the contact angle are relevant factors in a Stokes flow model if the capillary number is of the order of 1 or less.

The modelling of a moving front of a Newtonian fluid with surface tension and a no-slip condition results in a singular problem at the contact line [10, 11, 13]. No-slip and a moving contact line are kinematically compatible, but give rise to a multi-valued velocity. The velocity at the contact line will be discontinuous, the stress tensor thus becomes unbounded and unbounded forces are needed for the motion of the fluid at the contact line. There are two types of solutions to this singularity problem: the use of molecular dynamic modelling [20, 21, 30] and modification of the continuum mechanics model. The former is useful if one is interested in effects on molecular scale, but the latter is more practical for studying macro-scale effects.

Several modifications to the continuum mechanics models can be made. The most common one is the relaxation of the no-slip condition, which can be justified from several arguments. One assumption is that the fluid is not fixed to the solid, but moves with a (non)-linear friction over the surface [11, 12, 14, 16, 17, 18, 22, 24]. Another explanation for linear slip is that it originates from the rolling motion of the fluid over a rough surface [15].

Another modification to the continuum mechanics model is the elimination of the contact line by assuming a precursor film [3]. Copley *et al.* [8] demonstrated that the second assumption is actually not valid for glass. A third modification would be abandoning the Newtonian character of the fluid [28, 32]. A final modification would be the introduction of a surface tension gradient as a result of thermodynamics [27]. The latter two modifications result in quite complicated numerical models. Moreover, all modifications involve some unknown parameter.

Dussan V. [12] has shown that in models using slip the macro-scale flow depends on the slip parameter only, not on the actual formulation of the slip. Boender *et al.* [6] have calculated the shape of the meniscus from a (known) angle of the surface at some distance from the solid while ignoring the region of a few *nm* from this point to the contact line. From these results it can be concluded that any model could be adequate for the description of the macro-scale flow. Knowing this and not being interested in the flow at *nm* scale, we allow ourselves to use a simple linear slip model, which is the easiest to implement of all modifications mentioned above.

The linear slip condition we use corresponds to a friction linear in the velocity of the fluid. The friction force has to be in balance with the tangential forces on the fluid surface, i.e.

$$(\sigma \mathbf{n}) \cdot \mathbf{t} = \beta \mathbf{u} \cdot \mathbf{t} = (\mu / \lambda) \mathbf{u} \cdot \mathbf{t}, \tag{4.3}$$

with s the stress tensor, **t** and **n** the tangential and normal directions on the interface respectively, β the slip coefficient and λ the slip length, which is usually between 1 and 100 nm. Since the fluid cannot move through the boundary with the solid we also have the boundary condition

$$\mathbf{u} \cdot \mathbf{n} = 0. \tag{4.4}$$

In literature there is no common agreement on how the contact angle at a moving contact line behaves. One of the problems is the fact that the dynamic contact angle is not well defined. Experimental and numerical investigations in the neighbourhood of the contact line show that the surface of the fluid surface undergoes rapid changes near the contact line up to *nm* scale [6, 25]. An interesting conclusion, given by Boender [6], is that the value of the contact angle (at 1 nm from the solid surface) is dominant when the velocity is low. The dynamic contact angle is then close to the static value, and the value of the contact angle is of little importance at higher velocities when viscous forces dominate. Considering this and the fact that we are mainly interested in the mathematical model for a micrometer-scale flow, we will base our model, like most researchers, on a contact angle that equals the static contact angle.

However, the prescription of a fixed contact angle is not an easy task. It requires the velocity of the free surface to be constant near the contact line. In stationary moving boundary flows this is not a problem, because the whole surface is moving with a constant velocity. Solutions for these problems can be found with iterative approximation of the surface shape, given the position of the contact line [1, 9, 24]. For an instationary contact line the position is a priori unknown and the velocity of the free surface is not constant. Therefore we will use another approach to prescribe the contact angle, which has also been used by Bach and Hassager [1].

The static contact angle can be expressed in terms of a force using Young's equation [35]

$$\gamma \cos\theta_S = \gamma_{GS} - \gamma_{LS} = F_s. \tag{4.5}$$

Here θ_s represents the static contact angle, γ_{GS} and γ_{LS} are the surface tension on the gas-solid and liquid-solid interface and F_S the resulting force on the contact line. We now assume that the force working at a moving contact line equals the

force on a static contact line. Numerical results (§4.3) will show that the contact angle obtained with this force and linear slip in fact equals the static contact angle. When using a finite element method, the force on the contact line results in a natural boundary condition, while a fixed contact angle would result in an essential boundary condition. The former are much easier to handle.

4.2 Finite Element Formulation

In contrast to the previous problem we shall solve 'the drop on the solid plate' problem by a FEM. For non-isothermal situations, where we are really interested in, we believe the latter method to have a larger versatility.

For the solution of the Stokes equation we use a finite element method based on the following weak formulation:

$$\int_\Omega -\mu\left(\nabla\mathbf{u}+(\nabla\mathbf{u})^T\right):\nabla\mathbf{v}\,d\Omega+\int_\Omega p\nabla\cdot\mathbf{v}\,d\Omega+\int_\Gamma \mathbf{f}\cdot\mathbf{v}\,d\Gamma=0, \tag{4.6}$$

$$\int_\Omega(\nabla\cdot\mathbf{u})q\,d\Omega=0, \tag{4.7}$$

where $\mathbf{v}$ and q represent the test functions and $\mathbf{f}$ represents the natural boundary condition:

$$\mathbf{f}=\sigma\mathbf{n}, \tag{4.8}$$

which corresponds to a force on the surface of the fluid.

For the implementation of the surface tension we use a formulation described by Bach and Hassager [1]. Application of the Frenet formula

$$\frac{\mathrm{d}\mathbf{t}}{\mathrm{d}s}=\kappa\mathbf{n} \tag{4.9}$$

and partial integration of the weak formulation of the surface tension force results in the formulation

$$\begin{aligned}\int_{s_0}^{s_1}\mathbf{f}_\gamma\cdot\mathbf{v}\,\mathrm{d}s&=\int_{s_0}^{s_1}\left(-P_{ext}+\kappa\gamma\right)\mathbf{n}\cdot\mathbf{v}\,\mathrm{d}s\\&=-\int_{s_0}^{s_1}P_{ext}\mathbf{n}\cdot\mathbf{v}\,\mathrm{d}s-\gamma\int_{s_0}^{s_1}\mathbf{t}\cdot\frac{d\mathbf{v}}{ds}\mathrm{d}s+\gamma[\mathbf{v}\cdot\mathbf{t}]_1-\gamma[\mathbf{v}\cdot\mathbf{t}]_0\,,\end{aligned} \tag{4.10}$$

which can easily be implemented in a finite element model.

The advantage of this formulation is that the surface does not have to be smooth ($S\in C^0$). Another advantage is that the last two terms on the right-hand side describe a force on the edges of a surface which can be used to implement the contact angle as mentioned above in §4.1.

The problem defined above is the stationary case. The reduction to a stationary situation is allowed since the inertial effects can be neglected. Actually our problem is quasi-stationary, as the boundary is moving. For the time evolution of the drop we use the following equation for the displacement,

$$\dot{\mathbf{x}} = \mathbf{u}. \tag{4.11}$$

Here $\dot{\mathbf{x}}$ is the velocity of the boundary and $\mathbf{u}$ is the velocity of the fluid at the boundary. For the time integration (4.11) we refer to §3.2.

For the discretization of the problem we have used a Galerkin formulation and triangular Taylor-Hood elements with quadratic approximation of the velocity and linear pressure. This element satisfies the Babuška-Brezzi condition, is accurate and simple to implement. Moreover we did not want to use a penalty method, because the introduced artificial compressibility might give unrealistic solutions, due to the large variation in pressure near the contact line.

Every time step a completely new mesh is generated. The time required for this is acceptable compared to the time needed to build the matrix and solve the linear equations. It is less than 15% of the total time. The system of equations is solve by means of a LU-decomposition.

We have implemented the problem using the finite element package Sepran [26]. The mesh generation is done by an updated version of the mesh generator of this package which can handle large differences in element size without problems.

4.3 Numerical investigation of a model of an axisymmetric drop

We have chosen to simulate a drop similar to the one used by Hocking and Rivers [17] in their calculations and observations. This is a drop of glass with a radius $r_0 = 10^{-5}$ *m*. The temperature is kept constant at 800°C. The viscosity at this temperature $\mu = 10^5$ Ns/m^2. The surface tension $\gamma = 0.30$ *N/m*. The force on the contact line, $F_S = 0.295$ *N/m*, corresponds to a stationary contact angle of 10°. We did not vary this contact angle like Hocking, because a variation in the contact angle of 5° gives a variation in the contact line force less than 2% only. This would only give a significant variation in the solution near equilibrium, which would not be attained in our computations.

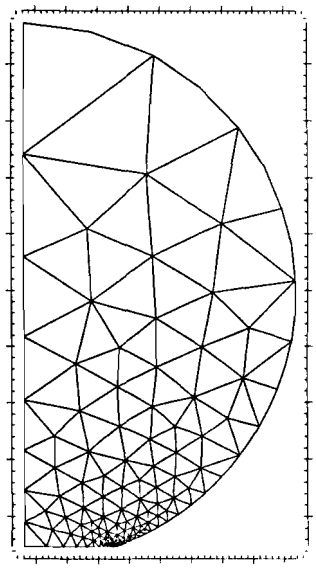

Figure 4:
mesh of the drop.

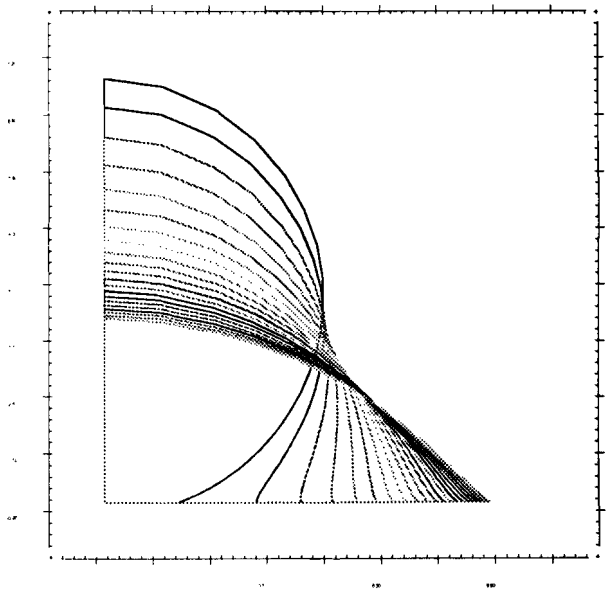

Figure 5: evolution of the drop in 10 time units.

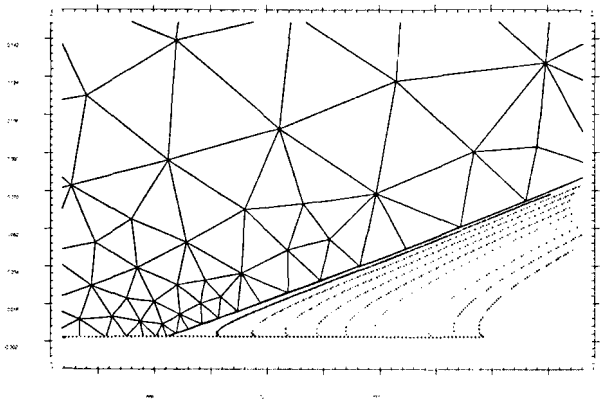

Figure 6: evolution of the surface near the contact line during 0.02 time units.

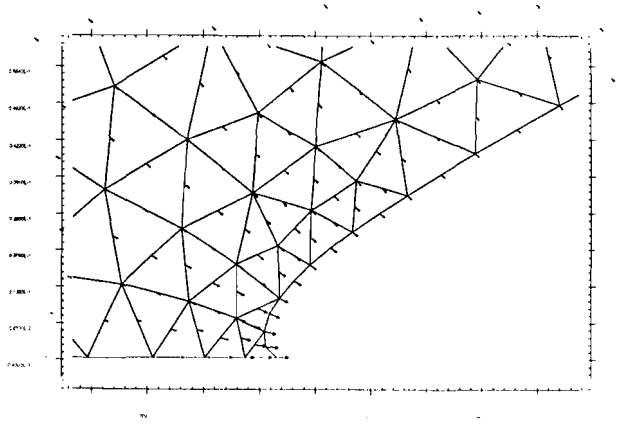

Figure 7: velocity field near the contact line.

Figure 4 shows the finite element mesh used in the computations. Figure 5 shows the evolution of the drop, with slip length $\lambda = 10^{-6}\, m$, during 10 time units. A close-up of the contact line region during the first 0.02 time units is given in figure 6. This figure illustrates that in this region the shape of the surface does not vary much after a very short transitional period. This already shows that the evolution of the drop involves two time scales, i.e. there is a time scale in the evolution, the initial contact line movement, which is much shorter than the time scale of interest, the evolution of the drop. As explained in section 2 this effect is introduced by the small elements on the surface.

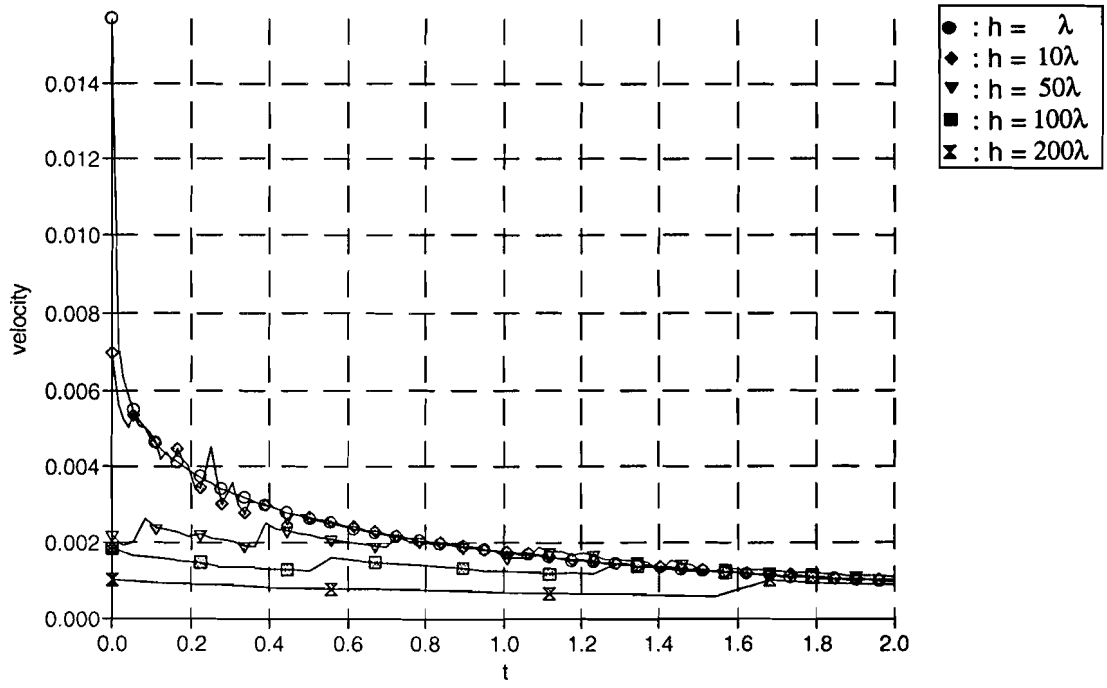

Figure 8: contact line velocity as a function of the element size on the contact line.

The influence of the use of larger elements on the velocity of the contact line is shown in figure 8. The wiggles present in this figure are due to small variations in the size of the elements during the evolution of the geometry. They are not a result of an instability in the time integration, which has been checked very carefully. From these results show that small elements are needed for an accurate solution of the evolution of the drop. This can be understood from looking at the velocity field (figure 7). The velocity is nearly constant in this region except for the solid surface where the velocity decreases exponentially, with a characteristic length comparable to the slip length (figure 9). The use of elements larger than the slip length results in a poor approximation of the velocity. However, the error introduced in the velocity near the contact line results in an acceptable error for an element size up to 50 times the slip length. Larger element sizes give a significant error in the evolution of the drop.

The microscopic contact angle in the discretized case, the angle at the corner of the element at the contact line, is shown in figure 10. One can see that for elements with a size equal to the slip length the microscopic contact angle corresponds to the static contact angle. For larger elements this is clearly not true, although the velocity is well approximated (figure 8).

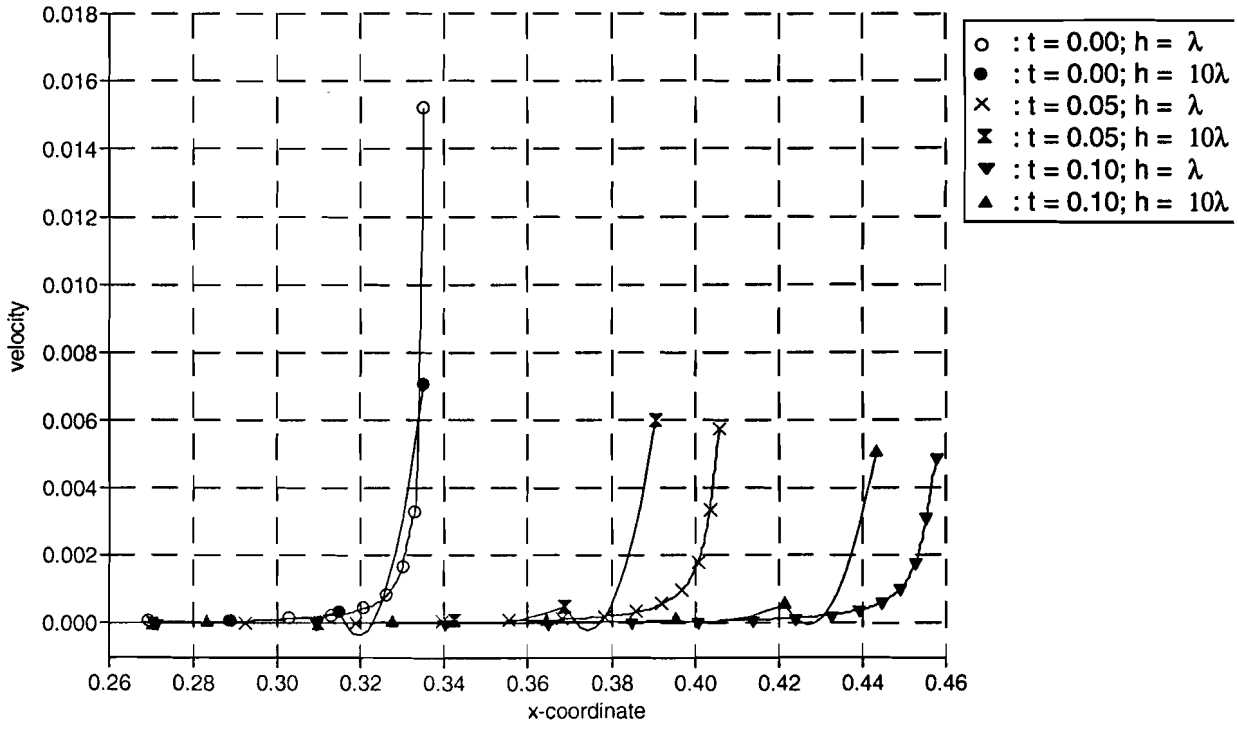

Figure 9: velocity of the fluid at the boundary with the solid.

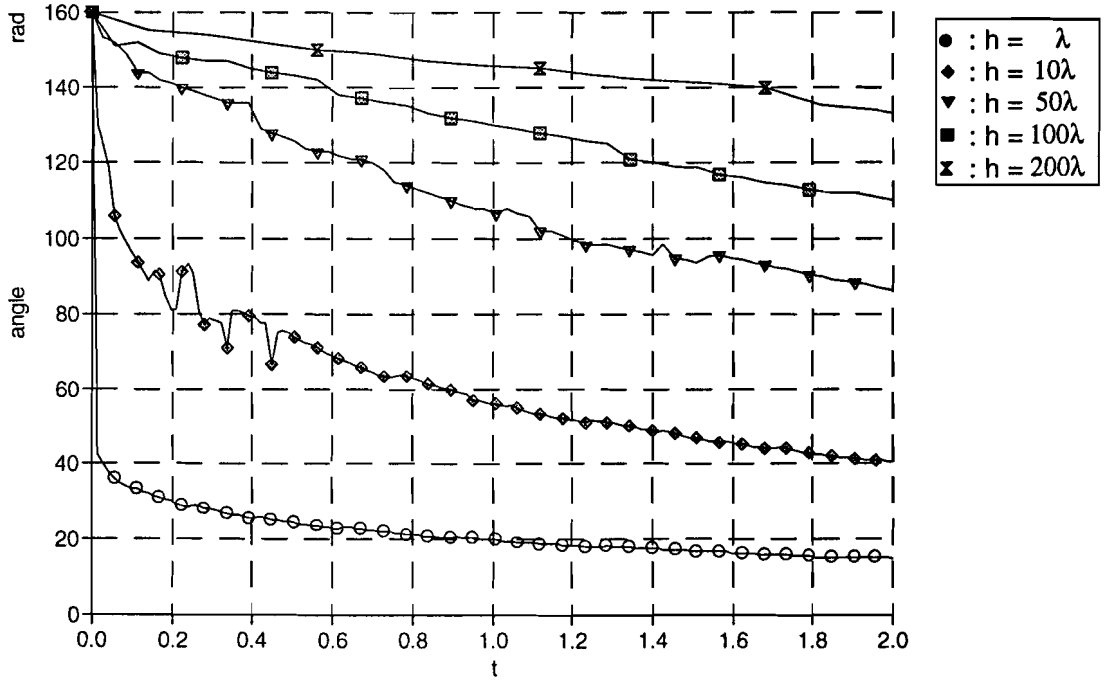

Figure 10: microscopic contact angle in the time for different element sizes.

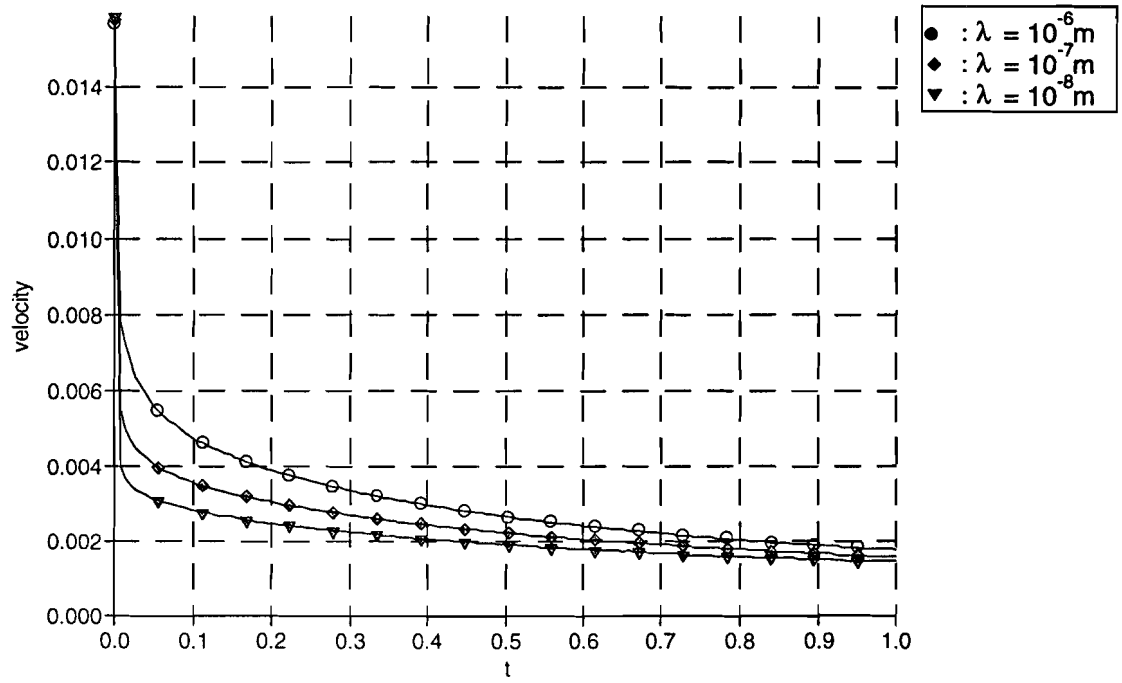

Figure 11: variation velocity as function of the slip length.

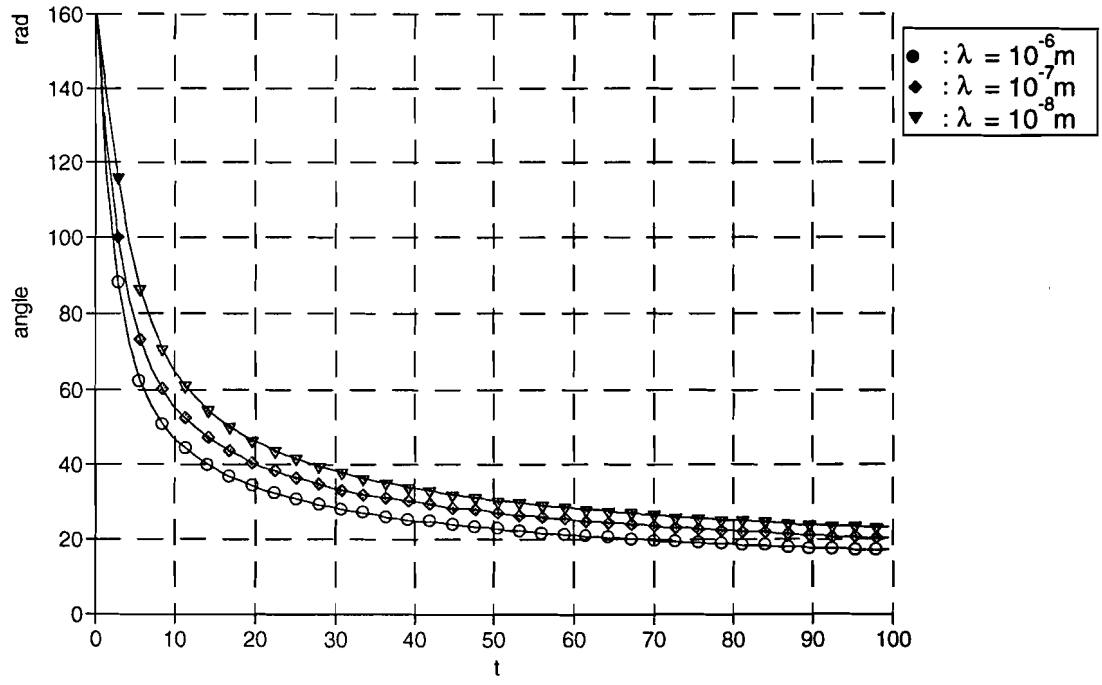

Figure 12: evolution of the angle of a spherical segment fitted on the drop for different slip lengths.

The velocity of the contact line also depends on the slip length as can be seen in figure 11. The slip length λ has been chosen 10^{-6}, 10^{-7} and 10^{-8} m respectively. To compare our results with the calculations of Hocking we have also computed the evolution of the shape of the drop as a function of the slip length (figure 12). The shape is expressed in the angle between the surface and a spherical segment fitted on the drop. The correspondence of our results with those of Hocking and Rivers is remarkable.

Acknowledgement

The authors wish to acknowledge useful discussions on the subject with Prof. G. de With.

References

[1] Bach P and Hassanger O: An algorithm for the use of the Lagrangian specification in Newtonian fluid mechanics and applications to free-surface flow, J Fluid Mech. 1985, vol 152, 173-190

[2] Banerjee PK: The Boundary Element Methods in Engineering, McGraw-Hill Book Company, London, 1994.

[3] Bascom WD, Cotting RL and Singleterry CR: Dynamic surface fenomena in the spontaneous spreading of oils on solids, In 'Contact Angles, Wettability and Adhesion' (RE Gould) p 355 Washington DC: Am Chem Soc.

[4] Becker AA: The Boundary Element Method in Engineering, McGraw-Hill Book Company, London, 1992.

[5] Beer G and Watson JO: Infinite Boundary Elements, Int. J. Numer. Meth. in Engng, 1989, 28, 1233--1247.

[6] Boender W, Chesters AK and Van der Zanden AJJ: An approximate solution of the hydrodynamic problem associated with an advancing liquid-gas contact line, Int. J. Multiphase Flow, vol 17, 661-676, 1991

[7] Brebbia CA and Dominguez J: Boundary Elements: An Introductory Course, CML Publications, Southampton, 1989.

[8] Copley GJ, Rivers AD and Smith R: Reappraisal of contact angle measurements of sodium and potassium silicate glasses on platinum in air, Glass Technology Vol 13 No 2 April 72, 50-53

[9] Cuvelier C: Some numerical methods for the solution of capillary free boundaries governed by the Navier-Stokes equations, reports of the faculty of mathematics and informatics 8769, technical university Delft, 1987.

[10] Davis SH: Contact-line problems in fluid mechanics, J of Applied Mechanics, dec 1983, vol 50, 977-982

[11] Dussan V. EB and Davis SH: On the motion of a fluid-fluid interface along a solid surface, J Fluid Mech. 1974, vol 65, 71-95

[12] Dussan V. EB: The moving contact line: slip boundary condition, J FLuid Mech 1976, vol 77 665-684.

[13] Dussan V. EB: On the spreading of liquids on solid surfaces: static and dynamic contact angles, Ann. Rev. Fluid Mech. 1979, 11:371-400

[14] Ford ML and Nadim A: Thermocapillary migration of an attachted drop on a solid surface, Phys Fluids 6, september 1994, 3183-3185

[15] Hocking LM: A moving liquid on a rough surface, J Fluid Mech 1976, vol 76, 801-817

[16] Hocking LM: A moving fluid interface. Part 2. The removal of the force singularity by a slip flow, J Fluid Mech 1977, vol 79, 209-229

[17] Hocking LM and Rivers AD: The spreading of a drop by capillary action, J Fluid Mech 1982, vol 121, 425-442

[18] Hocking LM: The spreading of drops with intermolecular forces, Phys. Fluids 6, 10 october 1994

[19] Hopper RW: Stokes Flow of a Cylinder and Half-Space Driven by capillarity, J. Fluid Mech., 1992, 243, 171--181.

[20] Koplik J, Banavar JR and Willemsen JF: Molecular dynamics of Poiseuille flow and moving contact lines, Phys Rev Letters, 1988, vol 60, 1282-1285

[21] Koplik J, Banavar JR and Willemsen JF: Molecular dynamics of fluid flow at solid surfaces, Phys. Fluids A 1(5) May 1989, 781-794

[22] Lacey AA: The motion with slip of a thin viscous droplet over a solid surface, Studies in applied mathematics, 67:217-230, 1982.

[23] Lee SH and Leal LG: The Motion of a Sphere in the Presence of a Deformable Interface. Part 2: Numerical study of the translation of a sphere normal to an interface, J. Colloid Interface Sci., 1982, 87, 81--106.

[24] Lowndes J: The numerical simulation of the steady movemnet of a fluid meniscus in a capillary tube, J. Fluid Mech 1980 vol 101 p 631-646

[25] Ngan CF and Dussan V. EB: On the nature of the dynamic contact angle: an experimental study, J Fluid Mech, 1982 vol118, p 27-40

[26] Sepran, Finite Element Toolbox, Ingenieursbureau Sepra, Leidschendam (Netherlands), 1993

[27] Shikhmurzaev YD: The moving contact line on a smooth solid surface, Int. J. Multiphase Flow, vol 19, pp 589-610, 1993.

[28] Simmons JH and Simmons CJ: Nonlinear visous flow in glass forming, Ceramic Bulletin, vol 68 no 11, 1989.

[29] Simonis F, NCNG-Glass course, Handbook for the Dutch Glass Production (in Dutch), TNO-TPD Glass Technology

[30] Thompson PA and Robbins MO: Simulations of contact line motion: slip and dynamic contact angle, Phys Rev Letters, august 1989, vol 63, 766-769

[31] Van de Vorst G.A.L. Modelling and Numerical Simulation of Viscous Sintering, PhD thesis, Eindhoven University of Technology, 1994.

[32] Weidner DE and Schwartz LW: Contact-line motion of shear-thinning liquids, Phys. Fluids 6 (11) Nov 94, 3535-3538

[33] West GD: On the resistance to the motion of a thread of mercury in a glass tube, Proc. Roy. Soc. A 86, 20, 1911-1912.

[34] De With G and Corbijn AJ: Fiber-on-Plate Experiments: Relaxation and Surface Tension, J. Appl. Phys., 1993. (Submitted).

[35] Young T: An essay on the cohesion of fluids, Philos. Trans. R. Soc. London 95:65-87, 1805

PREVIOUS PUBLICATIONS IN THIS SERIES:

Number	Author(s)	Title	Month
96–03	J.J.A.M. Brands	Asymptotics in order statistics	March '96
96–04	J.P.E. Buskens M.J.D. Slob	Prototype of the Numlab program. A laboratory for numerical engineering	March '96
96–05	J. Molenaar	Oscillating boundary layers in polymer extrusion	March '96
96–06	S.W. Rienstra	Geometrical Effects in a Joule Heating Problem from Miniature Soldering	April '96
96–07	A.F.M. ter Elst D.W. Robinson	On Kato's square root problem	April '96
96–08	H.J.C. Huijberts	On linear subsystems of nonlinear control systems	May '96
96–09	H.J.C. Huijberts	Combined partial feedback and input-output linearization by static state feedback for nonlinear control systems	May '96
96–10	A.F.M. ter Elst D.W. Robinson	Analytic elements of Lie groups	May '96
96–11	S.L. de Snoo R.M.M. Mattheij G.A.L. van de Vorst	Modelling of glass moulding, in particular small scale surface changes	July '96